Polarimetric bistatic radar scattering behavior of the ocean surface

Ahmad AWADA, Ali KHENCHAF and Arnaud COATANHAY
ENSIETA (Ecole Nationale Superieure des Ingenieurs des Etudes et Techniques d'Armement)
Laboratory E^3I^2 EA-3876 Brest France
Email: awadaah@ensieta.fr

***Abstract*— this paper points out the frequency dependence on the polarimetric radar scattering behavior of the ocean surface in the frequency range 1-18 GHz (L- to K_u-band). We treat this problem with a unifying scattering model named Small Slope Approximation (SSA) to evaluate the Normalized Radar Cross Section (NRCS). The calculations were made by assuming the surface-height spectrum of Elfouhaily *et al* for fully developed seas. In backscattering case, the frequency decreases causes an increasing in NRCS results. Yet, in the particular bistatic configuration (scattering along the specular direction), the opposite behavior takes place. The variations of the scattering azimuth relative to wind vector have no influence on the NRCS results along the specular direction, while in backscattering configuration it is not the case. Results were analyzed in monostatic case as well as in bistatic case for different sea states and polarization ones.**

I. INTRODUCTION

Radar Signals frequency value represents a key parameter in remote sensing applications. The choice of this value depends on the exploring target. Normally, ocean remote sensing applications are operated in L-, C-, X- and K_u-bands because wavelengths in these bands are most significant in remote sensing of the sea surface. Therefore, both radar backscatter and radiometric measurements have been proposed for determining the speed of the winds at the ocean surface. Since 1960, the scientific communities in this domain concept many aircraft measurement programs to provide quantitative information on the parametric behavior of the electromagnetic scattering coefficient (often called normalized radar cross section) σ^0 of the ocean. We can quote the Naval Research Laboratory (NRL) experiments [1] in which measurements were obtained as a function of polarization, incidence angle, and azimuth angle using pulse radars operating at 0.4, 1.2, 4.5, and 8.9 GHz. Other aircraft measurements [2] were also performed by the National Aeronautics and Space Administration, Johnson Space Center (NASA-JSC) using a fan-beam Doppler radar operating at 13.3 GHz. More recently, there is a new up to date to these measurements especially in K_u- and C-bands [3] [4]. It must be noted that ocean-scattered Global Positioning System (GPS) signals (L-band) become used as a remote sensing tool [5] in particular, to predict the wind vector over ocean surface [6]. The computed result for σ^0 along the specular direction is of major interest to bistatic sensing of the scattered signal from the GPS. It must be noted that recently bistatic and multistatic radar systems operating from air-borne and space-borne platforms received a renewed interest for its advantages in remote sensing of land and ocean surfaces [7]. These applications require the development of accurate models to predict the radar scattering from such surfaces. For ocean surface we can use the Two-scale model (TSM) [8] the integral equation model (IEM) [9], the Small slope approximation (SSA) [10], and the weighted curvature approximation WCA [11]. In this study the SSA model is used to treat the bistatic scattering from the ocean surface. This model is a unifying theory that could reconcile small perturbation method (SPM) and Kirchhoff approximation (KA) without introducing roughness scale division parameter. It can be applied to an arbitrary wavelength, provided that the tangent of grazing angles of incident/scattered angles radiation sufficiently exceeds RMS slopes of roughness. So, by using the SSA model, the purpose of this paper is to present a numerical study of the polarimetric bistatic radar scattering behavior of the ocean surface as a function of emission signals frequency in both monostatic and bistatic cases.

In the following section we recall briefly the SSA theoretical development and we point out the scattering dependence on the keys parameters. Section III deals with the sea surfaces characteristics: physical and geometrical. The fourth section is devoted to numerical simulations of the behavior of scattering by the ocean surface for monostatic case in first time, then in bistatic case. The last section summarizes the paper and presents some suggestions.

II. THEORETICAL SCATTERING FORMULATION

Wave scattering by rough surfaces is an important issue in diverse areas of science such as measurements in medicals, optics, geophysics, communications and remote sensing. Approximate models are still a necessity due to the insurmountable numerical complexity of the realistic scattering problems. Even today's machines cannot cope with the enormous amount of computing demand in the case of rigorous numerical calculations of the most general three-dimensional electromagnetic wave scattering from dielectric multi-scale surfaces such as ocean surface. We can refer to [12] which is the latest critical and up-to-date survey of the approximate models. Geometrical configuration adopted to resolve the wave-scattering problem from the sea surface is given in figure 1.

SSA, first introduced in [10], starts from an ansatz based on the invariance properties of the Scattering Amplitude (SA).

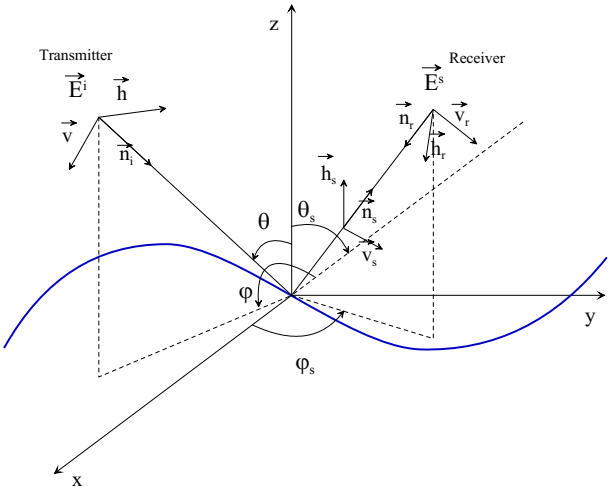

Fig. 1. Geometrical configuration for the wave-scattering from sea surface

Performing a horizontal or vertical translation $\boldsymbol{d}$ affects the latter by a phase shift $exp(-i(\boldsymbol{k}-k_0)\cdot\boldsymbol{d})$ or $exp(-i(q-q_0)\cdot\boldsymbol{d})$, so a solution is sought in the form where $\boldsymbol{k}_0, q_0$ are horizontal and vertical projections of the wave vector of an incident wave, and $\boldsymbol{k}, q$ are appropriate components of the wave vector of scattered wave.

$$S(\boldsymbol{k},\boldsymbol{k}_0) = \int \exp[-i(\boldsymbol{k}-\boldsymbol{k}_0)\cdot\boldsymbol{r} - i(q-q_0)h(\boldsymbol{r})] \times \Phi\left[\boldsymbol{k},\boldsymbol{k}_0,\boldsymbol{r},h\right]\frac{\mathrm{d}\boldsymbol{r}}{(2\pi)^2} \quad (1)$$

where Φ is some functional that contains the explicit dependence on the surface. The unknown Φ is obtained by performing a functional Taylor with respect to the Fourier transform $\hat{h}$ and imposing coefficients that give consistency with SPM as $h \to 0$. In practice, only the first two orders are tractable; the higher orders become far too intricate. At first order in the slope (SSA1) we have [13]

$$S_1(\boldsymbol{k},\boldsymbol{k}_0) = \frac{2(q\ q_0)^{1/2}}{q_k+q_0} B_1(\boldsymbol{k},\boldsymbol{k}_0)\frac{1}{(2\pi)^2} \times \int \exp[-i(\boldsymbol{k}-\boldsymbol{k}_0)\cdot\boldsymbol{r} - i(q-q_0)h(\boldsymbol{r})]d\boldsymbol{r} \quad (2)$$

with the corresponding cross section

$$\sigma_1(\boldsymbol{k},\boldsymbol{k}_0) = \frac{4qq_0}{(q+q_0)^2}\left|B_1(\boldsymbol{k},\boldsymbol{k}_0)\right|^2\frac{1}{(2\pi)^2} \times \int \exp[-i(\boldsymbol{k}-\boldsymbol{k}_0)\cdot\boldsymbol{r}]L(q+q_0;\boldsymbol{r})d\boldsymbol{r} \quad (3)$$

where the recentered characteristic function of the height difference is introduced as in [14]:

$$L(q+q_0;\boldsymbol{r}) := \langle\exp[-iq(h(\boldsymbol{r})-h(\boldsymbol{0})]\rangle - |\langle\exp[-iq(h(\boldsymbol{r})]\rangle|^2 \quad (4)$$

In the particular case of a Gaussian process $h(\boldsymbol{r})$, this expression assumes the well-known form:

$$L(q;\boldsymbol{r}) = \exp\left(-\frac{q^2}{2}D(\boldsymbol{r})\right) - \exp\left(-q^2\left\langle h^2\right\rangle\right) \quad (5)$$

where $D(\boldsymbol{r}) = \left\langle|h(\boldsymbol{r})-h(\boldsymbol{0})|^2\right\rangle$ is the structure function of the process. The second order in the slope (SSA2) is given by

$$S_2(\boldsymbol{k},\boldsymbol{k}_0,\boldsymbol{\xi}) = S_1(\boldsymbol{k},\boldsymbol{k}_0) - \frac{(q\ q_0)^{1/2}}{2i(q+q_0)}\frac{1}{(2\pi)^2} \times \int e^{(-i(\boldsymbol{k}-\boldsymbol{k}_0)\cdot\boldsymbol{r}-i(q+q_0)h(\boldsymbol{r}))}M(\boldsymbol{k},\boldsymbol{k}_0,\boldsymbol{\xi})\hat{h}(\boldsymbol{\xi})e^{i\boldsymbol{\xi}\cdot\boldsymbol{r}}\mathrm{d}\boldsymbol{\xi}\mathrm{d}\boldsymbol{r} \quad (6)$$

for some matrix $M(\boldsymbol{k},\boldsymbol{k}_0,\boldsymbol{\xi})$ that does not depend on the roughness, namely

$$M(\boldsymbol{k},\boldsymbol{k}_0,\boldsymbol{\xi}) = B_2(\boldsymbol{k},\boldsymbol{k}_0,\boldsymbol{k}-\boldsymbol{\xi}) + B_2(\boldsymbol{k},\boldsymbol{k}_0,\boldsymbol{k}+\boldsymbol{\xi}) -2(q+q_0)B_1(\boldsymbol{k},\boldsymbol{k}_0) \quad (7)$$

Here B_1 and B_2 are matrices describing the mutual influence of the different polarizations and depend on the physical problem under consideration. Explicit expressions for it can be found in [15]. In this study we treat the sea surface scattering problem. The Fourier transform of the roughness $\hat{h}$ is defined by

$$\hat{h}(\boldsymbol{\xi}) = \frac{1}{(2\pi)^2}\int \exp(-i\boldsymbol{\xi}\cdot\cdot\boldsymbol{r})h(\boldsymbol{r})d\boldsymbol{r} \quad (8)$$

The cross-section σ_2 associated with SSA2 is much more involved. For a stationary centered Gaussian process $h(\boldsymbol{r})$ with the correlation function $C(\boldsymbol{r})$, where $C(\boldsymbol{r}) = \langle h(\boldsymbol{0})h(\boldsymbol{r})\rangle$, it is given by

$$\sigma_2(\boldsymbol{k},\boldsymbol{k}_0) = \sigma_1(\boldsymbol{k},\boldsymbol{k}_0) + \sigma_{12}(\boldsymbol{k},\boldsymbol{k}_0) + \sigma_{22}(\boldsymbol{k},\boldsymbol{k}_0) \quad (9)$$

with ($\Re$ is the real part and $\overline{M}$ the conjugate)
σ_{12} and σ_{22} can be written in following forms:

$$\sigma_{12}(\boldsymbol{k},\boldsymbol{k}_0) = \frac{qq_0}{4(q+q_0)^2}\frac{1}{(2\pi)^2}\Re\int e^{-i(\boldsymbol{k}-\boldsymbol{k}_0)\cdot\boldsymbol{r}}L(q+q_0;\boldsymbol{r}) \times \int(1-e^{i\boldsymbol{\xi}\cdot\boldsymbol{r}})\hat{C}(\boldsymbol{\xi})\overline{B_1}(\boldsymbol{k},\boldsymbol{k}_0)\overline{M}(\boldsymbol{k},\boldsymbol{k}_0,\boldsymbol{\xi})\mathrm{d}\boldsymbol{\xi} \quad (10)$$

The relative magnitude of the first- and second- order terms depends on the roughness and the dielectric constant. In particular, the correction of the second term becomes negligible as the dielectric constant decreases. It can actually be checked [14] that $|(\boldsymbol{k},\boldsymbol{k}_0,\boldsymbol{\xi})/B_1(\boldsymbol{k},\boldsymbol{k}_0,\boldsymbol{\xi})|$ goes to zero as $\epsilon \to 1$, forcing the ration $|1-S_2/S_1|$ to zero as well.
and

$$\sigma_{22}(\boldsymbol{k},\boldsymbol{k}_0) = \frac{2qq_0}{q+q_0}\frac{1}{(2\pi)^2}\int e^{-i(\boldsymbol{k}-\boldsymbol{k}_0)\cdot\boldsymbol{r}}L(q+q_0;\boldsymbol{r}) \times \int e^{i\boldsymbol{\xi}\cdot\boldsymbol{r}}\hat{C}(\boldsymbol{\xi})\left|M(\boldsymbol{k},\boldsymbol{k}_0,\boldsymbol{\xi})\right|^2\mathrm{d}\boldsymbol{\xi} \quad (11)$$

To avoid the computational complexity in the SSA2 and accepting a small margin of correction (1 dB) [16], we will present numerical results by using SSA at first order in the next section for both monostatic and bistatic configurations.

To highlight scattering dependence on the key parameters (wave components, sea surface range, $\cdots$), we write the NRCS with SSA1 for an isotropically rough surface where equation (3) can be simplified as in our paper [17]:

$$\sigma_{\alpha\alpha_0}(\boldsymbol{k},\boldsymbol{k}_0) = 2\left|\frac{2q_k\ q_0}{q_k+q_0}B_{\alpha\alpha_0}(\boldsymbol{k},\boldsymbol{k}_0)\right|^2 \cdot \int_0^\infty \{e^{-\kappa[\rho(0)-\rho(r)]} - e^{-\kappa\rho(0)}\}J_0(Kr)rdr \quad (12)$$

where $\kappa = (q_k + q_0)^2$.
α, α_0 corresponds to the polarization of scattered and incident plane wave respectively. To illustrate the effective parameters which can be selected under a given system and geometric condition, we plot the integrand evaluation in equation (12) for scattering configuration along the specular direction at an incident angle equal to $60°$ and wind speed of 4 m/s.

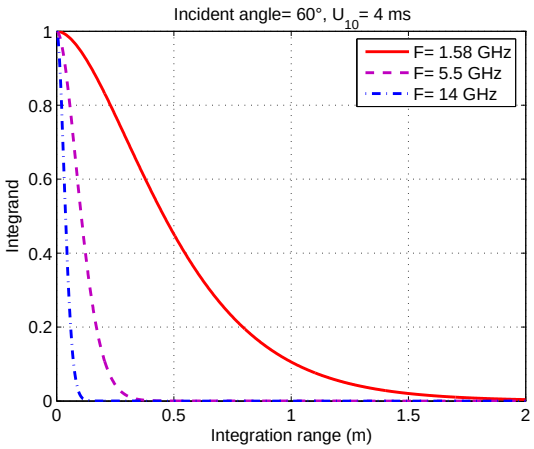

Fig. 2. Integrand evaluation of equation (12) for scattering along the specular direction for three frequencies 1.58, 5.5 and 14 GHz corresponding, respectively to L-, C- and K_u-band radar

Figure 2 shows that the effective surface parameters selected to explain scattering problem (backscattering or bistatic) at L-band cannot be used to explain scattering at K_u-band.

III. Sea surface modeling

Studying the scattering problem from the ocean surface requires modeling of the surface. In this context, present section deals with the key physical (*dielectric constants*) and geometrical characteristics (*spectrum or correlation function*) of the ocean surface.

A. Physical characteristics

Water molecule is a polar molecule. The dielectric response to frequency has a relaxation property. It is dependent on the temperature and salinity.

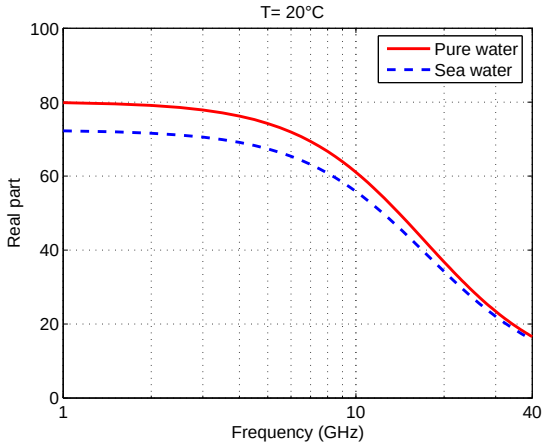

(a) Real part

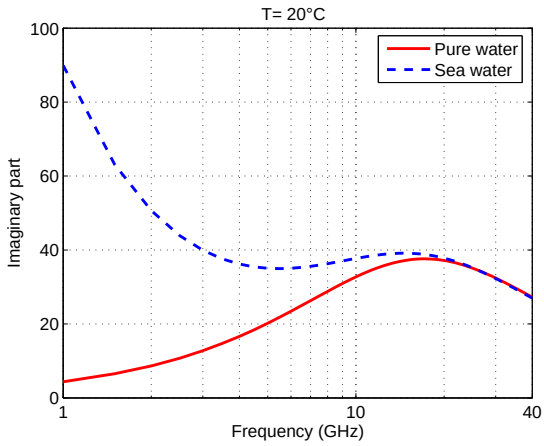

(b) Imaginary part

Fig. 3. The dielectric constants of pure and sea water (Salinity=35ppm) versus microwave frequency, (a) real part and (b) imaginary part

The dielectric constants of pure and sea water versus microwave frequency are shown in figure 3. Due to the large value dielectric constants of water, the waters such as ocean and rivers have high reflectivity and low emissivity. Part (b) shows clearly the important scope on the imaginary part between pure and sea water in the frequency range between 1 to 20 GHZ. On the other hand real part of the dielectric constant is less sensitive to salinity variations as shown in part (a) of the same figure.

B. Geometrical characteristics

Computing of the NRCS requires knowledge of either sea spectrum or sea height autocorrelation function which is obtained from the Fourier transform of the spectrum. In literature, there is many models to describe this surface. we quote the Pierson spectrum [18], the Apel spectrum [19], and the Elfouhaily one [20]. In the simulations in present paper we will use the Elfouhaily model (unified spectrum), which was recently developed based on available field and wave-tank measurements, and which is backed up with strong physical arguments contrary to other spectra which are mostly empirical.

It is important to note that this model was developed without any relation to remote-sensing data. Its agreement with the slope model proposed by Cox and Munk [21] and with actual remote sensing data make it a credible model. Elfouhaily *et al* assume a directional spectrum $S(K,\psi)$ defined in polar coordinates as

$$S(K,\psi) = S(K)f(K,\psi) \tag{13}$$

where

$$S(K) = (B_L + B_H)/K^3 \tag{14}$$

and

$$f(K,\psi) = [1 + \Delta(K)\cos(2\psi)]/2\pi \tag{15}$$

In (13), $S(K)$ denotes the non-directional spectrum (isotropic part) modulated by the $f(K,\psi)$ spreading function. In (14), B_L and B_H are the respective contributions from low (gravity waves) and high (cappliray waves) wavenumbers. ψ is the azimuthal angle measured with respect to the mean wind direction. The factor $\cos(2\psi)$ in (15) is responsible to return the spectrum symmetric compared to the wind direction axis. Figure 4-a illustrates the Elfouhaily spectrum isotropic part behavior versus the wavenumber for three wind speeds U_{10}=$\{5,\ 10,\ \text{and}\ 15\}$ m/s. For the simulations, a fully developed sea is assumed which is similar to take an inverse wave age Ω equal to 0.84. From this figure, it is clear that the spectral peak increases with wind speed and shifts towards the gravity waves. The vertical lines are placed at wavenumbers responsible for Bragg backscatter $K_B = 2K\sin\theta$ at $\theta = 50°$ for frequencies of 1.58 and 14 GHz, corresponding, respectively, to L- and C-band radar.

In figure 4-b we plot corresponding correlation function based on Elfouhaily spectrum. The sea autocorrelation behavior is clearly a moderately narrow band process and hence the oceanic covariance is not at all describable by a Gaussian correlation function, as has sometimes been assumed in the past. This behavior is similar to the one obtained by Apel [19] by using his model. Note that there is significant range of negatives values not presented in most correlation functions of land surfaces. It can actually be checked [17] that in particular cases of NRCS calculations there is a significant range of the negative part to be integrated over (for illustration see figure 2).

All these surface representations presented in this section will be a key feature, when estimating the NRCS of the sea surface in both monostatic and bistatic cases object of the next section.

IV. Numerical analysis

This section would be dedicated to numerical examples to analyze the polarimetric radar scattering behavior of the ocean surface especially as a function of emission frequency. Results will be presented in monosatatic configuration then in bistatic one.

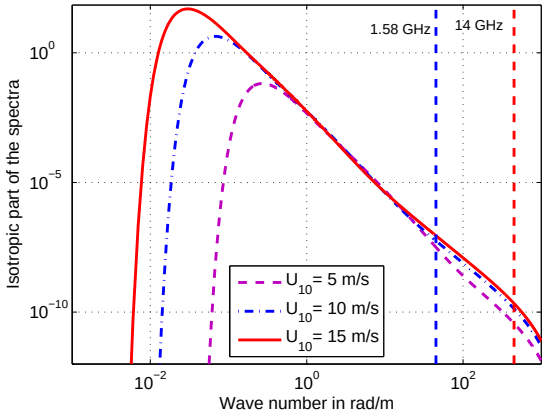

(a) Real part

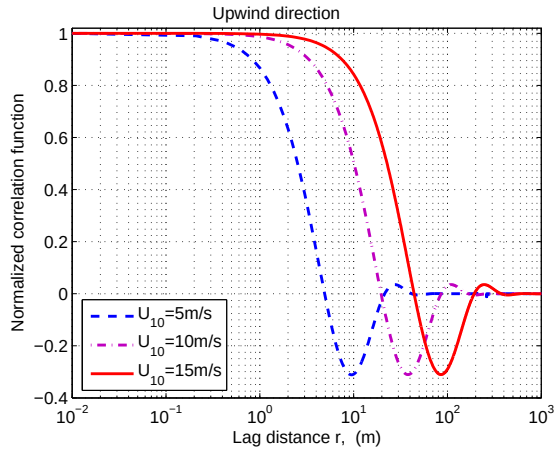

(b) Imaginary part

Fig. 4. (a) Isotropic part of the Elfouhaily spectrum [20] versus the wavenumber for three wind speeds of 5, 10 and 15 m/s. The vertical lines are placed at wavenumbers responsible for Bragg backscatter $K_B = 2K\sin\theta$ at $\theta = 50°$ for frequencies of 1.58 and 14 GHz, and (b) the corresponding normalized correlation function in upwind direction

A. Frequency dependence on backscattering configuration

The backscattering configuration is obviously of utter importance in many applications as classic radars, satellite SAR images and other electromagnetic sensors. Therefore, the numerical results in scientific references are almost solely given for backscattering problems.

That is the reason why first we present our numerical evaluations in this context.

Plots of backscattering coefficients versus frequency are shown in figure 5. Part (a) is the vertically polarized case, and part (b) is the horizontally polarized one. We are validated these simulations by comparing it with experimental data published in [18].

In examining the curves in this figure, one still gets the overall impression that radar backscatter does increase with wind speed. An obvious trend indicated by theory is that wind dependence decreases with decrease in frequency.

Anisotropic scattering characteristics predicted by the SSA

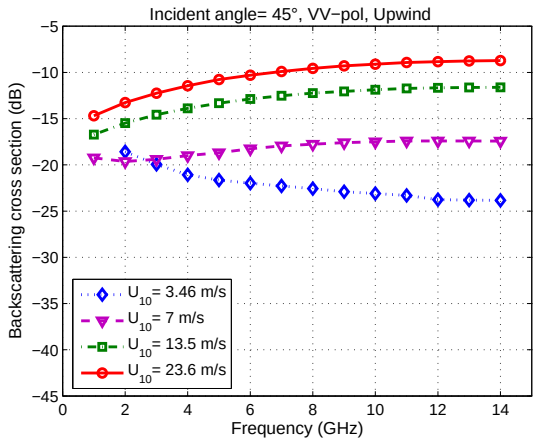

(a) VV polarization

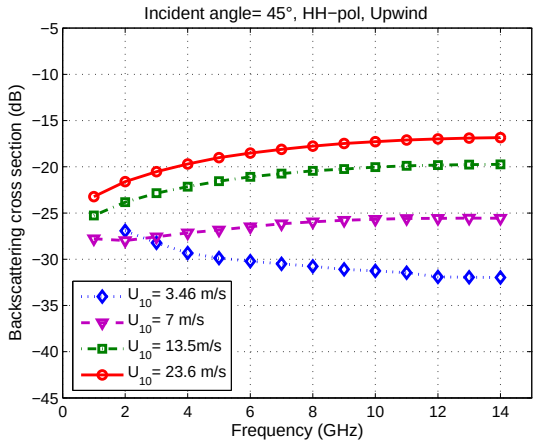

(b) HH polarization

Fig. 5. Variations of backscattering coefficient versus frequency for various wind speeds in upwind case, (a) VV polarization and 45○ incidence angle (b) HH polarization and 45○ incidence angle

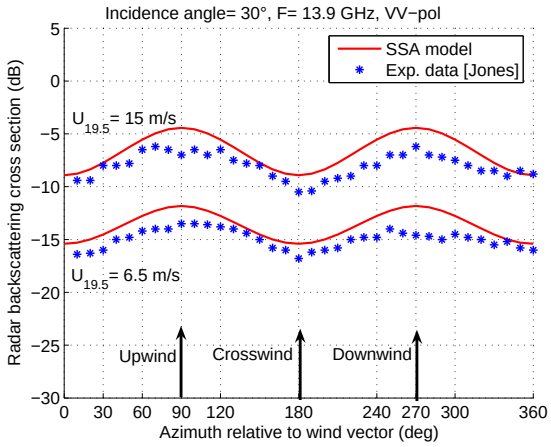

(a) VV polarization

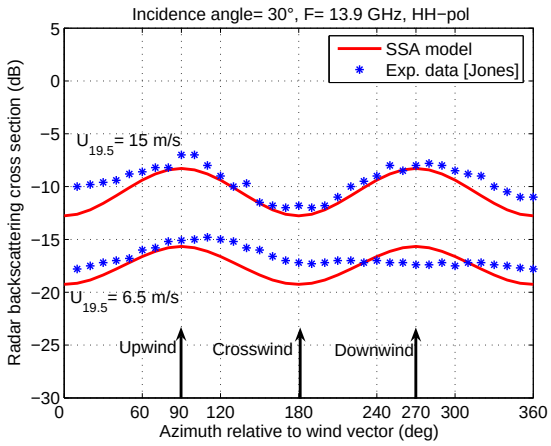

(b) HH polarization

Fig. 6. Radar backscattering cross sections predicted by the SSA for 30° incidence versus the azimuthal angle compared to experimental data published in [22]

model for two wind speeds $U_{19.5}$= 6.5 and 15 m/s are shown in figure 6. The abscissa is the radar azimuth relative to croswind direction. Again, we can note that the larger backscattering coefficients (σ^0) values are associated with the higher wind speed. The anisotropic scattering characteristic is a quasi-sine of twice the azimuth angle curve with the peaks in the upwind and downwind directions and the minima in the crosswind.
By comparing the theoretical curves and the experimental data published in [22], it is clear that there is a good agreement between them, with a small difference of about 2 dB. Since the Elfouhaily *et al* [20] sea spectrum, used in numerical calculations, was assumed to obey Gaussian statistics, the upwind and downwind directions results are equally predicted. Finally, these simulations illustrate the potential of obtaining both wind speed and wind direction from multi-look (azimuth) radar measurements of the oceans's surface.

In figure 7 theoretical radar backscattering cross section versus the azimuth angle are shown with frequency as a parameter. It is seen that change in σ^0 results between crosswind and upwind directions decreases with decrease in the incident frequency. Note that the predicted curves become flatter with lower radar frequency, because a rough surface appears smoother at larger wavelength.

In the next paragraph we will present the numerical results obtained in the particular bistatic configuration : scattering along the specular direction.

B. Frequency dependence on bistatic configuration

After the monostatic results and analysis, we study in present section the dependence frequency on the normalized bistatic cross section (NBCS) by numerical results simulated by using the SSA model in different configurations and sea states. We note that a deeply comparison between the SSA and TSM model in bistatic configuration was made in [23].

Similar to the monostatic study in the previous section, we present in figure 8 variations of the NBCS along the specular direction for 40° incidence angle as function of the radar signals frequency values. This simulation is obtained for three wind speeds 5, 10 and 15 m/s and in upwind direction,

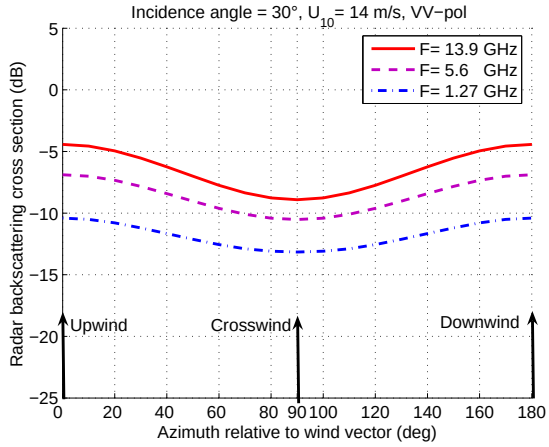

(a) VV polarization

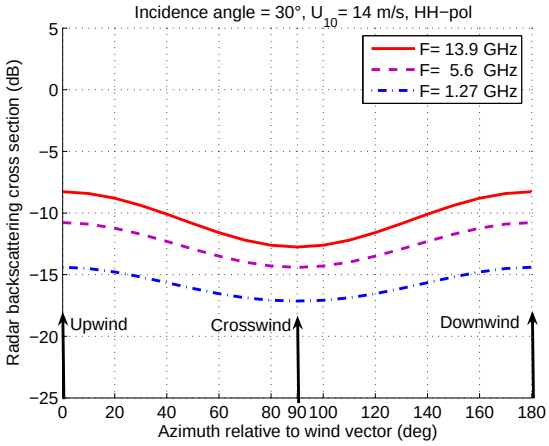

(b) HH polarization

Fig. 7. Radar backscattering cross sections predicted by the SSA versus the azimuthal angle at L-, C-, and K_u-band for $30°$ incidence and two wind speeds, (a) VV-polarization and (b) HH-polarization

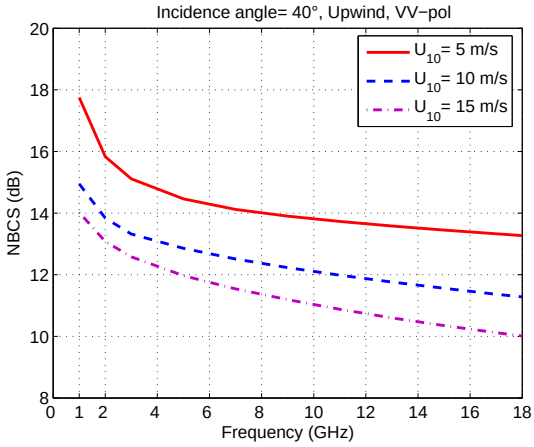

(a) VV polarization

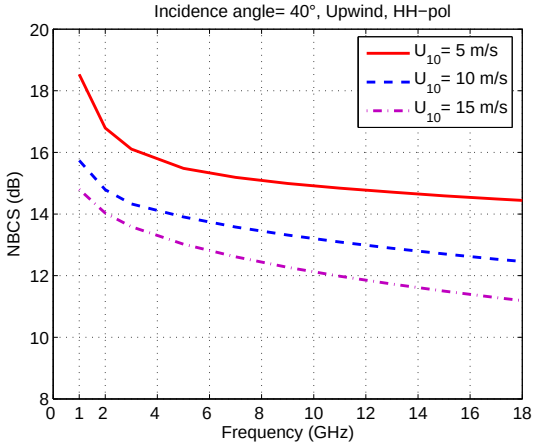

(b) HH polarization

Fig. 8. Frequency dependence on the scattering along the specular direction for $40°$ incidence angle at three wind speeds $\{5,\ 10,\ 15\text{m/s}\}$, (a) VV-polarization and (b) HH-polarization

part (a) shows the VV-polarization results and part (b) the HH-polarizations ones. As is apparent in figure 8 the NBCS values decrease with increasing of the frequency values which is the opposite behavior of the backscattering case seen in the previous section (see figure 5). It must be noted that the difference between NRCS values at L- and K_u-band is of about 5 dB in this scattering case along the specular direction.

Figure 9 shows the NBCS variations along the specular direction versus the incident angle $0° - 80°$ for frequencies of 1.58, 5.5 and 14 GHz, corresponding, relatively to L-, C- and K_u-band radar. The wind speed is fixed to 4 m/s and the upwind direction is under consideration.

In examining curves in figure 9 several items of importance may be deduced. First, for both VV- and HH-polarizations the NBCS values are quasi constant in the incidence region $[0° - 60°]$. This behavior can be able a significant result in exploring the sea clutter. Second, for VV-polarization in part (a) beyond $60°$ there is an important decreasing in NBCS results. on the other hand, in part (b), the horizontally polarized scattering coefficient continues to rise with incident angle up to $80°$ except for L-band frequency. Beyond $70°$, in this particular case (F= 1.58 GHz), the coefficient turns back down. This down turn is due to integration into negative correlation region (see figure 4-b).

With he same parameters as in figure 9 we plot simulations results at wind speed of 10 m/s in figure 10.

By comparing the curves of figure 9 and those of 10, we can conclude the only remark that for L-band the down turn in the HH-polarization curve vanishes, this is simply because the negative correlation region does not include in NBCS calculations at wind speed of 10 m/s (see figure 4-b).

Finally, we present in figure 11 the NBCS results along the specular direction at an incidence angle of $50°$ for three frequency bands. Unlike the backscattering configuration, it is clear in this bistatic configuration the wind direction independence on the NBCS result where it is constant for all azimuth directions.

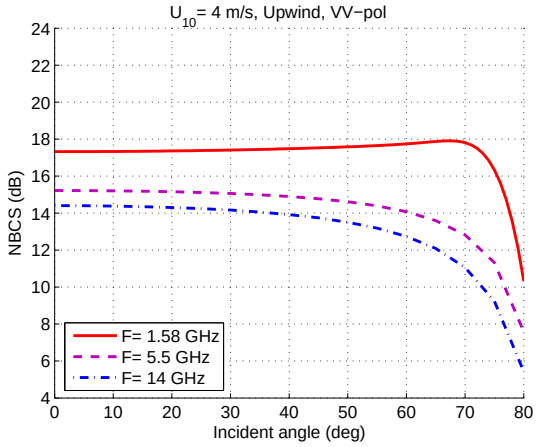

(a) VV polarization

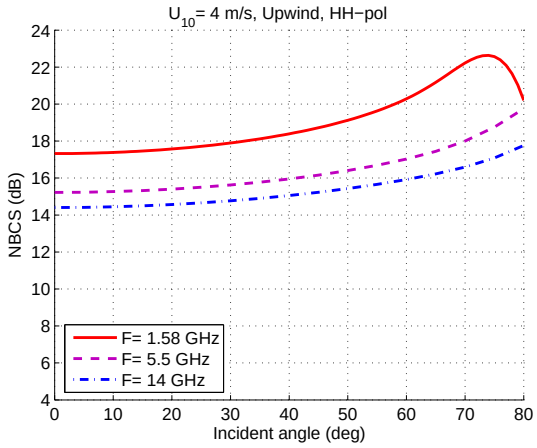

(b) HH polarization

Fig. 9. NBCS variations along the specular direction for L-, C- and K_u-band at a wind speed of U_{10}=4 m /s, (a) VV-polarization and (b) HH-polarization

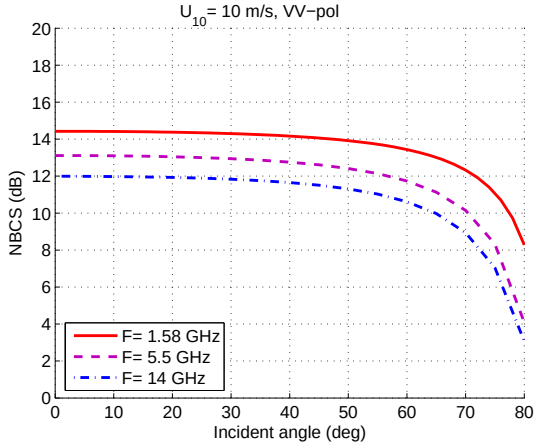

(a) VV polarization

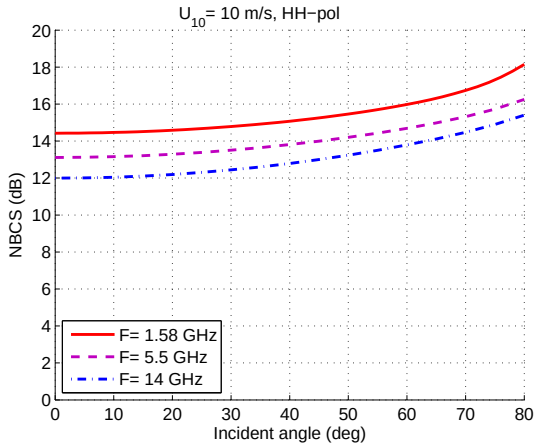

(b) HH polarization

Fig. 10. NBCS variations along the specular direction for L-, C- and K_u-band at a wind speed of U_{10}=10 m /s, (a) VV-polarization and (b) HH-polarization

V. Conclusion

In this paper we have studied the polarimetric radar scattering behavior of the ocean surface particularly as a function of the radar frequency value. After a rapid presentation of the unifying scattering model the SSA, the sea surface modeling is described by its physical (dielectric constant) and geometrical characteristics (spectrum or correlation function). The frequency dependence on all these parameters is discussed. As is the aim of this paper, a numerical evaluations of the NRCS in monostatic configuration in first time. From this part, it is seen that the dependence of wind direction becomes small when the emission frequency decreases. Then, in second time the numerical results are analyzed in the particular case of the bistatic case (the specular direction) versus the frequency value. As opposite to backscattering case, the NRCS in bistatic case (specular direction) decreases with the increasing of the radar frequency. For scattering large incident angles, the low radar frequency (L-band) becomes unexploitable signals in the sea scattering (specular direction) which limits the using of the adopted theoretical model at small wind speeds. The recently WCA model seems to be promising to improve some particular bistatic cases predicted with the SSA model which will be exploited in our future work.

References

[1] G. R. Valenzuela, M. B. Laing, and J. C. Daley, "Ocean spectra for the high frequency waves as determined from airborne measurements," *Journal of Marine Research*, vol. 29, no. 2, pp. 69–84, May 1971.

[2] K. Krishen, "Correlation of radar backscattering cross sections with ocean wave height and wind velocity," *J. Geophys. Res.*, vol. 76, no. 20, pp. 6528–6539, 1971.

[3] F. J. Wentz, "A model function for the ocean-normalized radar cross section at 14 GHz derived from NSCAT observations," *J. Geophys. Res.*, vol. 104, pp. 499–514, 1999.

[4] A. Bentamy, P. Queffeulou, Y. Quilfen, and K. Katsaros, "Ocean surface wind fields estimated from satellite active and passive microwave instruments," *IEEE trans. Geosci. Remote Sensing*, vol. 37, pp. 2469–86, 1999.

[5] J. Martin-Neira, C. Mavrocordatos, and E. Colzi, "Study of a constellation of bistatic radar altimeters for mesoscale ocean applications," *IEEE trans. Geosci. Remote Sensing*, vol. 36, pp. 1898–1904, 1998.

[6] Y. Huaizu, J. L. Garrison, G. Heckler, and Z. U. Zavorotny, "Stochastic voltage model and experimental measurement of ocean-scattered gps signal statistics," *IEEE trans. Geosci. Remote Sensing*, vol. 42, pp. 2160 – 69, 2004.

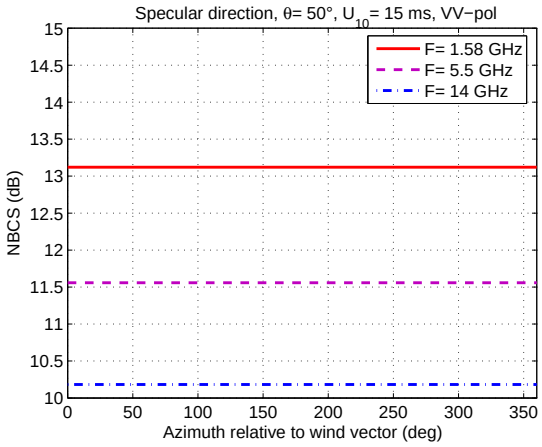

(a) VV polarization

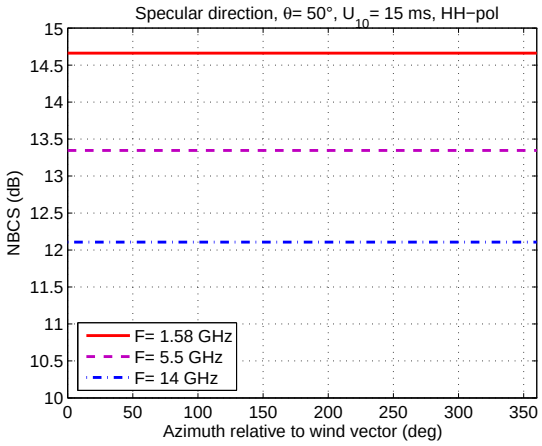

(b) HH polarization

Fig. 11. NBCS variations along the specular direction for L-, C- and K_u-band versus the the azimuthal angle for an incident angle of 50° at U_{10}=15 m /s, (a) VV-polarization and (b) HH-polarization

[7] V. U. Zavorotny and A. V. Voronovich, "Scattering of GPS signals from the ocean with wind remote sensing application," *IEEE trans. Geosci. Remote Sensing*, vol. 38, no. 2, pp. 951–964, 2000.

[8] A. Khenchaf, "Bistatic scattering and depolarization by randomly rough surfaces: application to the natural rough surfaces in X-band," *Waves Random Media*, vol. 11, pp. 61–89, 2001.

[9] A. K. Fung, *Microwave scattering and emission models and their applications*, A. House, Ed., Boston, 1994.

[10] A. G. Voronovich, "Small slope approximation in wave scattering from rough surfaces," *Sov. Phys. JETP*, vol. 62, pp. 65–70, 1985.

[11] T. Elfouhaily, S. Guignard, R. Awadallah, and D. R. Thompson, "Local and non-local curvature approximation: a new asymptotic theory for wave scattering," *Waves Random Media*, vol. 13, pp. 321–328, 2003.

[12] T. Elfouhaily and C. A. Guérin, "A critical survey of approximate scattering wave theories from random rough surfaces," *Waves Random Media*, vol. 14, pp. R1–R40, 2004.

[13] A. G. Voronovich, *Wave Scattering From Rough Surfaces (Springer Series on Wave Phenomena)*, Springer, Ed., Berlin, 1994.

[14] C. A. Guérin and M. Saillard, "On the high-frequency limit of the second-order small-slope approximation," *Waves Random Media*, vol. 13, pp. 75–88, 2003.

[15] A. G. Voronovich, "Small-slope approximation for electromagnetic wave scattering at a rough interface of two dielectric half-spaces," *Waves Random Media*, vol. 4, pp. 337–367, 1994.

[16] C. Bourlier, "Azimuthal harmonic coefficients of the microwave backscattering from a non-Gaussian ocean surface with the first-order SSA model," *IEEE trans. Geosci. Remote Sensing*, vol. 42, no. 11, pp. 2600–2611, 2004.

[17] A. Awada, A. Khenchaf, and A. Coatanhay, "Bistatic radar from an ocean surface at L-band," *in the proceedings of the IEEE Radar Conference*, Verona, NY, USA 2006.

[18] A. K. Fung and K. K. Lee, "A semi-empirical sea-spectrum model for scattering coefficient estimation," *IEEE Jou. Ocean. Engine.*, vol. 7, no. 4, pp. 166–176, 1982.

[19] J. R. Apel, "An improved model of the ocean surface wave vector spectrum and its effects on radar backscatter," *Journal. Geo. Res.*, vol. 99, no. C7, pp. 16,269–16,291, 1994.

[20] T. Elfouhaily, B. Chapron, K. Katsaros, and D. Vandemark, "A unified directional spectrum for long and short wind-driven waves," *J. Geophys. Res.*, vol. 102, no. C7, pp. 781–796, 1997.

[21] C. Cox and W. Munk, "Slopes of the sea surface deduced from photographs of sun glitter," *Bull. Scripps. Inst. of Oceanog.*, vol. 6, pp. 401–488, 1956.

[22] W. L. Jones, L. C. Schroeder, and J. L. Mitchell, "Aircraft measurements of the microwave scattering signature of the ocean," *IEEE trans. Antennas Propag.*, vol. AP-25, pp. 52–61, 1977.

[23] A. Awada, A. Khenchaf, A. Coatanhay, and M. Y. Ayari, "Comparison between small slope approximation and two scale model in bistatic configuration," *in The proceedings of the IEEE International Geoscience and Remote Sensing Symposium*, pp. 1341–1344, Seoul, Korea 2005.